processes

MDPI

Article

Thermal Stress Mechanism of Thermochemical Reactor of 5 kW Solar Simulator with Temperature Distribution as the Load Condition

Xing Huang [1], Yan Lin [1], Xin Yao [1,2,*], Yang Liu [3,*], Fanglin Gao [1] and Hao Zhang [4]

[1] College of Metallurgy and Energy, North China University of Science and Technology, 21 Bohai Street, Tangshan 063210, China; minthx@163.com (X.H.); ly12172018@163.com (Y.L.); 15137062679@163.com (F.G.)
[2] Tangshan Chuangyuan Fangda Electric Co., Ltd., Tangshan 063000, China
[3] Health Center, North China University of Science and Technology, Tangshan 063210, China
[4] School of Electrical Engineering and Automation, Harbin Institute of Technology, 92 West Dazhi Street, Harbin 15001, China; zh_hit@hit.edu.cn
* Correspondence: yaoxin_0129@163.com (X.Y.); liuyangineur@outlook.com (Y.L.); Tel./Fax: +86-0315-8805020 (X.Y. & Y.L.)

Abstract: In this paper, a solar thermochemical reactor is designed based on a 5 kW non-coaxial concentrating solar simulator, and a mathematical model is established for thermal calculations. The calculated temperature distribution is used as a load condition for thermal stress analyses. The model is used to study the influence of the solar simulator power, solar reactor inner wall material's emissivity, working pressure, gas inlet velocity, and thermocouple opening diameter on the thermal stress of the solar reactor. The results show that thermal stress increases with the increase in solar simulator power and the emissivity of the inner wall material in the solar reactor. The inlet velocity and working pressure have little effect on the thermal stress of the reactor and cannot prevent damage to the reactor. In the case of maintaining the diameter of the thermocouple at the front end of the reactor, increasing the diameter of the thermocouple inside the reactor leads to an increase in thermal stress around the reactor. Meanwhile, using a finer thermocouple can reduce the thermal stress inside the reactor and extend its service life, which will provide a foundation for designing practical industrial applications in the future.

Keywords: solar thermochemical reactor; temperature field; thermal stress; safety

Citation: Huang, X.; Lin, Y.; Yao, X.; Liu, Y.; Gao, F.; Zhang, H. Thermal Stress Mechanism of Thermochemical Reactor of 5 kW Solar Simulator with Temperature Distribution as the Load Condition. *Processes* **2024**, *12*, 1016. https://doi.org/10.3390/pr12051016

Academic Editor: Federica Raganati

Received: 8 April 2024
Revised: 29 April 2024
Accepted: 30 April 2024
Published: 16 May 2024

1. Introduction

At present, with China's proposal of a "dual carbon" goal, clean energy is receiving increasing attention from people [1]. The synthesis gas produced by a solar thermal chemical reactor using concentrated solar energy to drive high-temperature chemical reactions is a highly efficient and sustainable source of clean energy that has been widely promoted [2]. However, solar reactors need to create a high-temperature environment to achieve the activation energy required for these chemical reactions to occur. High-density solar radiation, uneven heating, and improper heating rates can all cause localized high temperatures in the solar reactor, resulting in stress concentrations and damage to the reactor [3]. Therefore, the phenomenon of thermal stress concentration in solar reactors is the most significant factor that affects the stability and lifespan of solar thermal chemical reactors.

In concentrated solar thermal technology, the incident solar energy is reflected by the reflector and focused on the solar receiver, where it is converted into thermal energy [4–6]. This thermal energy is supplied to the cavity for thermochemical reactions [7–11]. During this process, the phenomenon of thermal stress concentration is caused by the temperature gradients generated by localized high temperatures. Some domestic and foreign scholars have conducted relevant research on this phenomenon. In the early 1980s, Duke et al. [12,13]

and Bethea [14] first researched the service life of glass-based reflectors. They conducted outdoor tests at various locations, and their research revealed that the long-term reflectivity of the material surface is crucial to the lifespan of reflectors. During the same period, Boeing Engineering conducted durability testing on coated aluminum reflectors [15] and Paul et al. [16] conducted extensive research on polymer reflectors. Their results showed that applying a layer of polymer on the reflector increased its service life by up to twenty years. In fact, the early literature mainly studied the factors affecting the service life of three different reflectors exposed to various environments over an extended period of time. Segura et al. [17] summarized this aspect well but did not pay attention to other parameters, such as temperature, geometric shape, and thermal stress. In recent years, scholars have studied the effect of geometric shapes on the stress levels of solar thermochemical reactors. Daabo al. [18] utilized numerical simulation methods to investigate the cavity structure of solar receivers. By comparing three different cavity structures—spherical, cylindrical, and conical—the results showed that the conical receiver absorbed the highest radiation flux. The results showed that, among these three types of heat exchangers, the improved hemispherical heat exchanger generated the smallest equivalent stress and demonstrated the best safety and stability. In addition to the geometric shape, the placement position of the cavity reactor is also important. Therefore, Wang et al. [19] introduced an eccentric tube heat exchanger and studied the effect of eccentricity and inclination on the stress levels of the eccentric tube heat exchanger. The results showed that it is recommended than an eccentric tube heat exchanger with an optimal eccentricity and inclination of 90° be used as the tube heat exchanger for a groove condenser system. The literature above has comprehensively studied stress distribution in terms of structure and position, aiming to obtain the optimal geometric shape and position for reactors. Some scholars have also conducted in-depth research on reactor materials; Wang et al. [20], compared four different materials for solar energy absorbers: stainless steel, silicon carbide, aluminum, and copper. The results show that the effective thermal stress and total strain of solar energy absorbers made of stainless steel and copper materials are the highest and lowest, respectively. Therefore, copper solar collectors are safer. Although Wang et al. used high-thermal-conductivity materials to significantly reduce stress concentrations, they did not consider material corrosion. Therefore, Du et al. [21] proposed a composite solar heat collector with a thermal conductivity layer and a high-temperature protective layer. They selected two materials: a chromium nickel–iron alloy 718/nickel and 316 stainless steel/GRCop-84. The results showed that the design of the composite material could reduce the maximum thermal stress of the solar heat collector. Furthermore, as the pipe wall thickness and solar radiation intensity increase, the performance improvement becomes more significant. Hischier et al. [22] used 13 heliostats with incident powers ranging from 32 to 38 kW to study the thermal stress of a silicon-based cavity absorber at a height of 31 m on a solar tower. The results showed that adjusting the incident flux distribution and airflow cooling can minimize the temperature distribution to some extent and reduce thermal stress concentrations. In addition, the temperature gradient is a key factor that causes thermal stress in solar thermochemical reactors. Therefore, many efforts have been made to reduce the distribution of temperature differences by altering operating conditions. Chen et al. [23] studied the influence of parameters such as mass flow rate, inlet temperature, and irradiance on the mechanical performance of solar collectors to ensure their safe and efficient operation. The results showed that the thermal stress of a solar collector is directly proportional to its mass flow rate and irradiance, and inversely proportional to its inlet temperature. Bader et al. [3] developed a thermodynamic model for a 3 kW solar thermochemical reactor and solved it numerically to predict its temperature and stress distribution under static conditions. The results showed that the static safety factor of the reactor, as determined by Mohr's method, was acceptable. Additionally, the reactor demonstrated an ability to flexibly change its operating conditions. Zhang et al. [24] simulated the thermodynamic process of thermochemical reactors under high solar radiation and discussed the causes of thermal stress formation and the location of ceramic damage.

At present, most research has focused on the stress analysis of solar reflectors, solar heat absorbers, and solar cells, while there are few reports on the thermal stress analysis of solar thermochemical reactors. Solar simulators generate thermal stress due to temperature gradients. Therefore, the temperature field is utilized as a load condition in the finite element model of solar reactors, but there are no relevant reports on the parameters that may affect thermal stress, such as material reflectivity, solar power, gas inlet velocity, working pressure, and thermocouple diameter. The utilization of solar thermal chemical reactors to generate syngas can address the global energy demand and promote sustainable energy development. The phenomenon of thermal stress concentrations is an important factor that affects the stability and lifespan of reactors. Therefore, this article is based on a self-designed solar reactor that utilizes a 5 kW solar simulator, with temperature distribution as the load condition, to complete a thermal stress analysis using APDL. The influence of solar simulator power, the emissivity of the solar reactor's inner wall material, working pressure, gas inlet velocity, and the diameter of the thermocouple opening on solar reactor thermal stress is studied. A decrease in the thermal stress in solar reactors could extend their service life, laying the groundwork for developing feasible industrial applications in the future.

2. Geometric Model

Because thermal analysis is a prerequisite for thermal stress analysis, it is necessary to calculate the temperature field under various operating conditions. Figures 1 and 2 depict the contours of temperature distribution and velocity distribution in a solar reactor at a solar simulator power of 2.4 kW. It can be seen from Figure 1 that the high-temperature region under high-flux irradiation is mainly concentrated at the front end of the solar reactor. While ceramic insulation layers can withstand high-temperature conditions, such environments present challenges to their thermal stability [25]. The main reason for thermal stress concentrations is a temperature gradient; solar reactors with severe temperature fluctuations are more prone to ceramic damage at the front end [26]. Figure 2 illustrates the direction of the inlet gas flow and highlights the benefits of cooling the quartz window. The streamline is almost parallel to the inlet, quartz glass, and inner wall, which is not conducive to improving thermal stress.

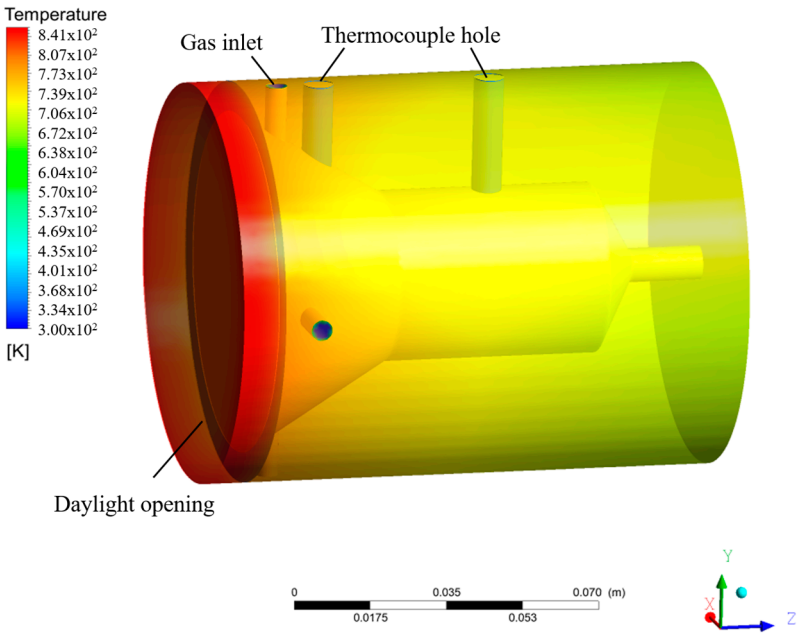

Figure 1. Temperature distribution contour map of solar reactor.

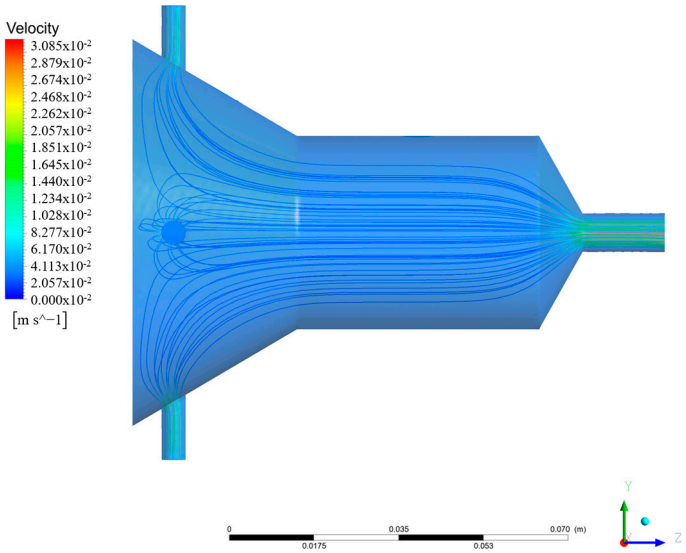

Figure 2. Velocity distribution contour map of solar reactor.

The high-temperature heat flux density of the solar simulator is generated in the interior of the solar reactor through the daylighting port for heating; the uneven heating inside generates temperature differences, resulting in thermal stress. To accurately analyze the thermal stress inside the solar reactor, APDL is utilized for a thermal stress analysis. Firstly, the thermal analysis of the solar reactor is conducted using Fluent. The temperature node information of the solid part of the solar reactor is then imported into APDL for the thermal stress analysis. In other words, the physical model and grid are obtained from Fluent. The thermal analysis of a solar reactor is equivalent to laying the foundation for a thermal stress analysis. Figure 3 shows the meshing model of a solar reactor with a temperature load in APDL.

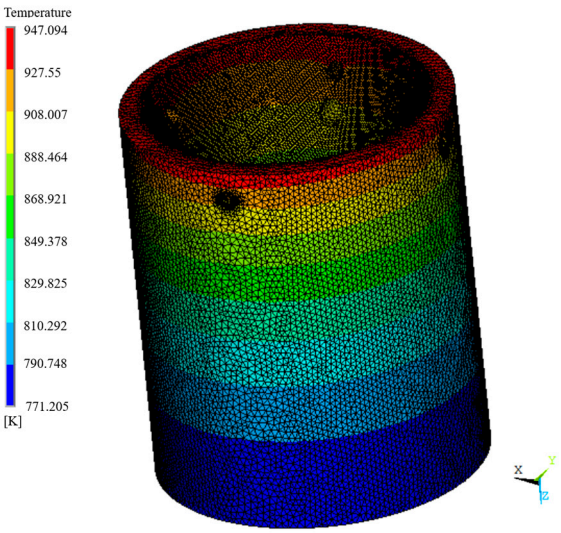

Figure 3. Thermal stress analysis model of solar reactor.

3. Mathematical Model

The problem of thermal stress caused by temperature changes requires the use of thermoelasticity. The method for solving the problem is the same as that of elasticity, which is studied from the perspectives of geometry, mechanics, and physics. The difference between the two is that, in thermoelasticity, the stress and strain are not only affected by external forces but also take into account the influence of temperature changes. Thermoelastic mechanics considers the stress and strain caused by temperature and external forces, which

are a superposition of the two. The governing equations of thermoelasticity in rectangular coordinates are expressed as follows [27]:

(1) The generalized Hooke's law of thermal stress:

$$\varepsilon_{x_i} = \frac{1}{2G}(\sigma x_i - \frac{\nu}{1+\nu}\Theta) + \alpha\Delta T \tag{1}$$

$$\gamma_{x_i x_j} = \frac{\tau_{x_i x_j}}{G}, i \neq j \tag{2}$$

In the formula, $G = \frac{E}{2(1+\nu)}$ is the shear elastic modulus (Pa); E is the Young's modulus (Pa); σ_{x_i} denotes the stress component (Pa) acting on the infinitesimal; ν represents Poisson's ratio; $\Theta = \sum \sigma_{x_i}$ is the volume stress (Pa); α denotes the linear thermal expansion coefficient (K^{-1}); ΔT indicates the temperature difference (K); τ indicates the shear stress (Pa); and γ denotes shear strain.

(2) The displacement equation of thermoelastic mechanics:

$$(\lambda_l + G)\frac{\partial e}{\partial x_i} + G\nabla^2 u_i - \beta\frac{\partial(\Delta T)}{\partial x_i} + X_i = 0 \tag{3}$$

where $e = \sum \varepsilon_{x_i}$ represents the volume strain; $\beta = \alpha(3\lambda_l + 2G)$ is the thermal stress coefficient (Pa K^{-1}); $\lambda_l = \frac{E\nu}{(1+\nu)(1-2\nu)}$ indicates the Lame coefficient (Pa); X_i denotes the component of unit volume force on the coordinate axis (N m^{-3}); and ∇^2 represents the Laplace operator.

(3) The coordination equation of thermoelasticity:

$$\nabla^2\sigma_{x_i} + \frac{1}{1+\nu}\frac{\partial^2\Theta}{\partial x_i} = -\alpha E\left[\frac{1}{1-\nu}\nabla^2(\Delta T) + \frac{1}{1+\nu}\frac{\partial^2(\Delta T)}{\partial x_i^2}\right] \tag{4}$$

$$\nabla^2\tau_{x_i x_j} + \frac{1}{1+\nu}\frac{\partial^2\Theta}{\partial x_i \partial x_j} = -\frac{\alpha E}{1+\nu}\frac{\partial^2(\Delta T)}{\partial x_i \partial x_j} - \left(\frac{\partial X_j}{\partial X_i} + \frac{\partial X_i}{\partial X_j}\right) \tag{5}$$

4. Load and Boundary Conditions

The thermal stress in the solar simulator is caused by its temperature gradient. Therefore, the temperature is used as the loading condition in the three-dimensional finite element model of the solar reactor. First, the temperature load needs to be obtained. This can be achieved through a thermal fluid–solid coupling simulation analysis using Fluent. Once the temperature load is obtained, it can be exported from Fluent and loaded into APDL. Then, other boundary conditions need to be set, such as specifying its material properties. Finally, various constraints are applied to different surfaces of the model to resolve the calculation. In addition to the temperature load, the thermal stress analysis of the solar reactor also takes into account the pressure and gravity of the fluid on the solid wall. Because the pressure of the solar reactor in this paper has little effect on its thermal stress, it is not considered. The pressure caused by gravity is negligible, so this paper only considers the influence of temperature load on the solar reactor.

5. Model Validation and Thermal Stress Analysis

5.1. Model Validation

The equivalent stress (Von Mises stress) in ANSYS APDL can not only clearly describe the stress changes in the model but also quickly identify the most critical location in the model. The stress analysis method used in this paper is equivalent stress analysis. This method was chosen due to the complexity of the structure, which requires transforming each principal stress into an equivalent stress to describe the stress concentration phenomenon [28]. The theory follows the fourth strength theory of materials, which states that the yield of materials is caused by their distortion energy density. In other words, when the

distortion density reaches the material's limit value, the model will experience the yield phenomenon. Although it is not possible to determine whether the ceramic is damaged, the location and sequence of the damage can be determined.

The strength condition of the fourth strength theory is

$$\sqrt{\frac{1}{2}\left[(\sigma_1-\sigma_2)^2+(\sigma_2-\sigma_3)^2+(\sigma_3-\sigma_1)^2\right]} \leq [\sigma] \quad (6)$$

In the formula, the allowable stresses of the material, σ_1, σ_2, σ_3, are the first, second, and third principal stresses.

In order to validate the accuracy of the model, the computational model proposed in this paper was used to calculate the model in Reference [24]. The calculation parameters are as follows: the power of the solar simulator is 10 kW, the inlet velocity is 0.005 m/s, and the pressure is one atmosphere. Figure 4a shows the simulation results for Von Mises stress. From the diagram, it can be seen that the model has four stress concentration positions (A, B, C, D), which are consistent with the reference. The most vulnerable position is A (13.17×10^3 MPa), which is only 6.64% different from the literature simulation results (12.35×10^3 MPa). It can also be inferred that the ceramic is prone to cracking at the junction of the four stress concentrations. This conclusion is supported by both the simulation results and experimental results found in the literature (Figure 4b). Therefore, this model can be utilized for thermal stress calculations.

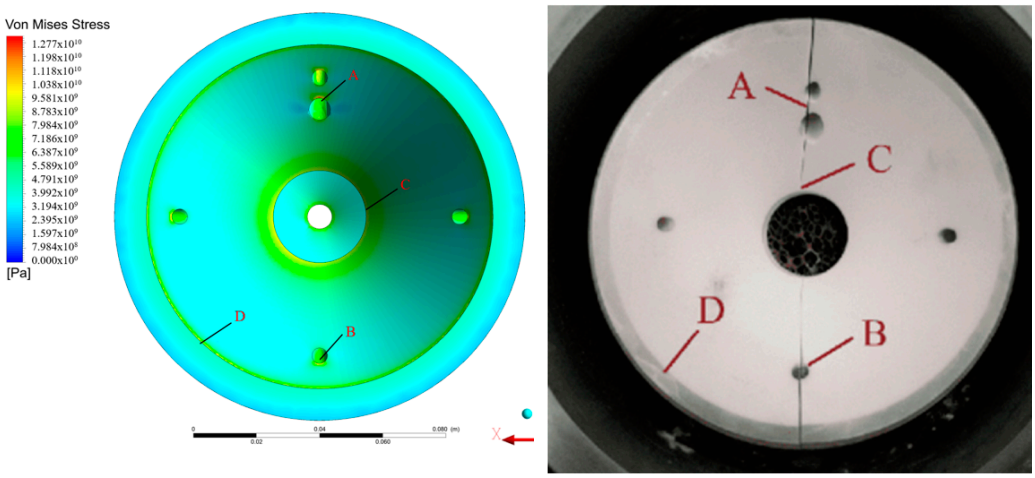

(**a**) (**b**)

Figure 4. The simulation results are compared with the literature. (**a**) Von Mises stress simulation results; (**b**) experimental results in the literature. (A: the inlet opening, B: the front thermocouple opening, C: aperture, D: the lighting opening).

5.2. Thermal Stress Analysis

Figure 5 illustrates the distribution of thermal stress in the solar reactor. The calculation parameters are as follows: the power of the solar simulator is 2.4 kW, the velocity at the gas inlet is 0.005 m/s, the temperature at the inlet is 300 K, and the working pressure is 0.1 MPa. It can be seen from the figure that thermal stress concentrations mainly occur at the front of the solar reactor and at the thermocouple opening located in the center of the porous area. From the contour map of thermal stress, it can be observed that the maximum thermal stress is mainly concentrated on the inner edge and areas surrounding the openings, such as the thermocouple opening (A, a), the front thermocouple opening (B), the inlet opening (C), and the lighting opening (D) situated at the center of the porous area of the solar reactor. The most vulnerable locations to damage are the thermocouple openings (A: 6.24×10^3 MPa) and the front thermocouple openings (B: 5.65×10^3 MPa) located in the center of the porous area of the solar reactor. If the thermal stress exceeds the ultimate

strength of the ceramic material, it will result in damage to the ceramic components of the solar reactor, thereby impacting its overall lifespan. Therefore, it is important to minimize thermal stress concentrations in order to prevent damage to the solar reactor and extend its service life.

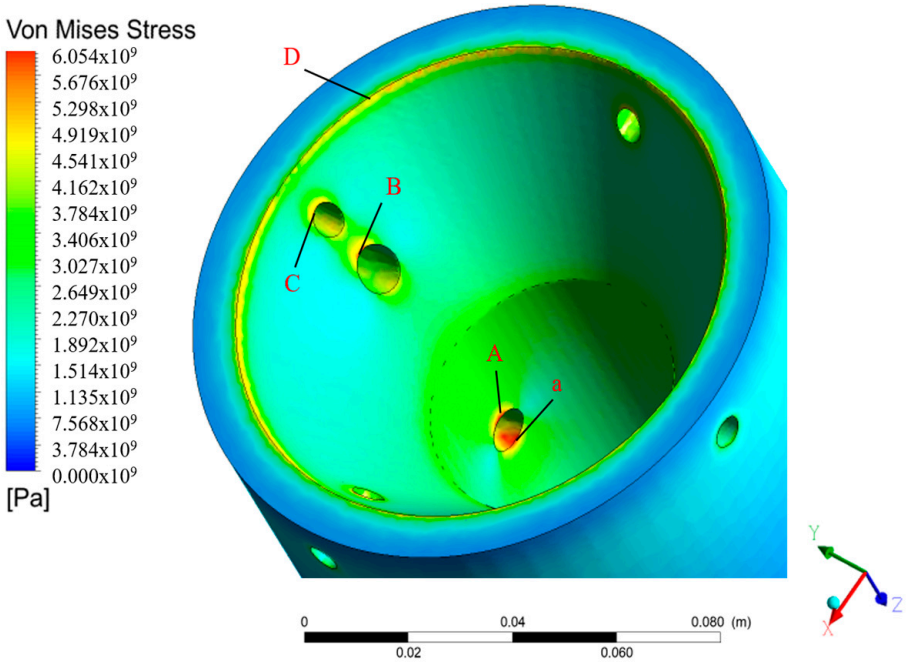

Figure 5. Thermal stress distribution cloud. (A, a: the thermocouple opening, B: the front thermocouple opening, C: the inlet opening, D: the lighting opening).

6. Results and Discussion

6.1. The Influence of Solar Simulator Power

Figure 6 illustrates the impact of various solar simulator powers on the thermal stress of solar reactors. The calculation parameters are as follows: a gas inlet velocity of 0.005 m/s, a gas inlet temperature of 300 K, a working pressure of 0.1 MPa, and a solar simulator power ranging from 1 to 5 kW. It can be seen from the figure that as the power of the solar simulator increases, the thermal stress at solar reactors A and B also increases. As the solar power increases, the temperature gradually decreases along the axis. This is primarily due to radiation heat loss at the wall, resulting in a rapid temperature decrease near the aperture [29]. The increase in power also leads to an excessive concentration of heat flow, resulting in temperature non-uniformity and exacerbating the thermal stress concentration [30]. When the power of the solar simulator increases from 1 to 5 kW, the thermal stress at point A increases from 4.69×10^3 MPa to 7.30×10^3 MPa, resulting in an increase of 2.61×10^3 MPa. Similarly, the thermal stress at point B increases from 4.10×10^3 MPa to 6.71×10^3 MPa, also increasing by 2.61×10^3 MPa. Figure 7 shows the cloud map of the thermal stress distributions in solar reactors under various solar simulator powers. It can be seen from the figure that increasing the power of the solar simulator leads to intensified thermal stress concentrations in the solar reactor. If the thermal stress exceeds the ultimate strength of the ceramic material, it will result in ceramic damage to the solar reactor and impact its operational lifespan. Therefore, after reaching the solar reactor's required temperature, the power of the solar simulator should be reduced as much as possible to minimize thermal stress concentrations.

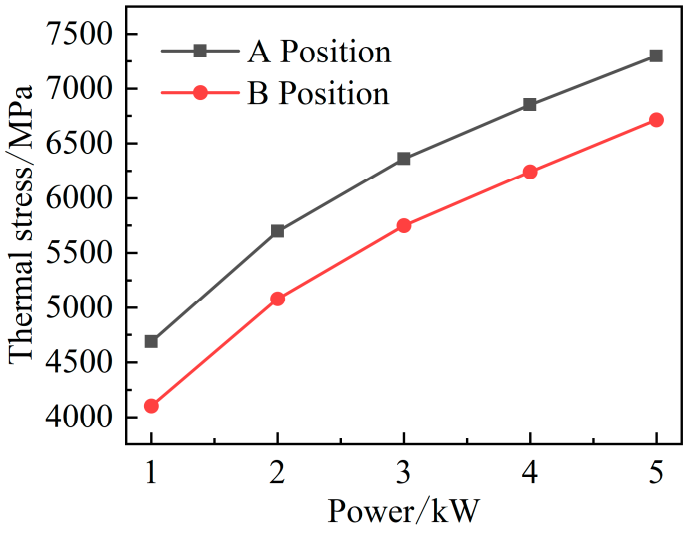

Figure 6. The influence of simulator power on the temperature distribution of the reactor centerline.

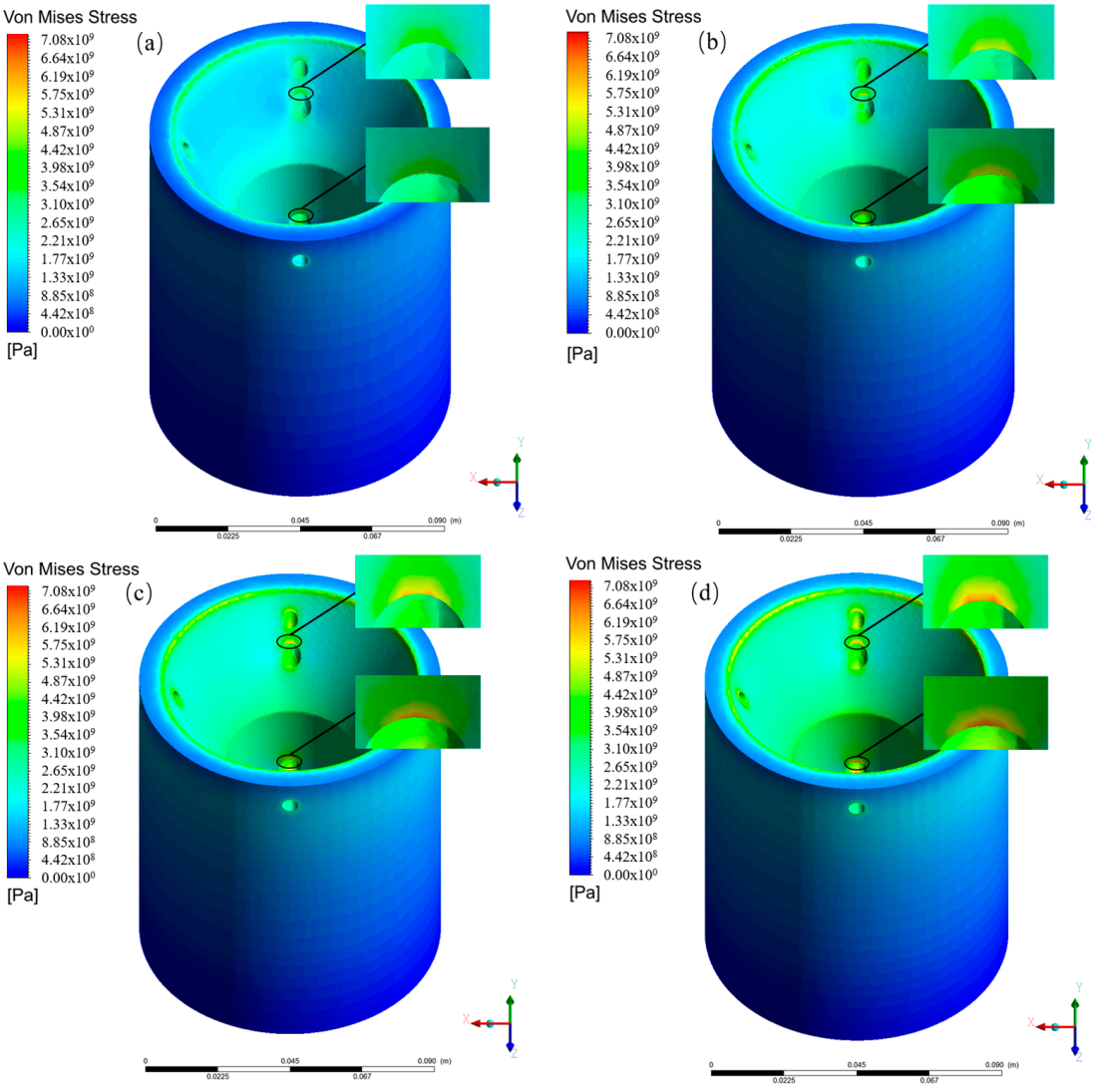

Figure 7. *Cont.*

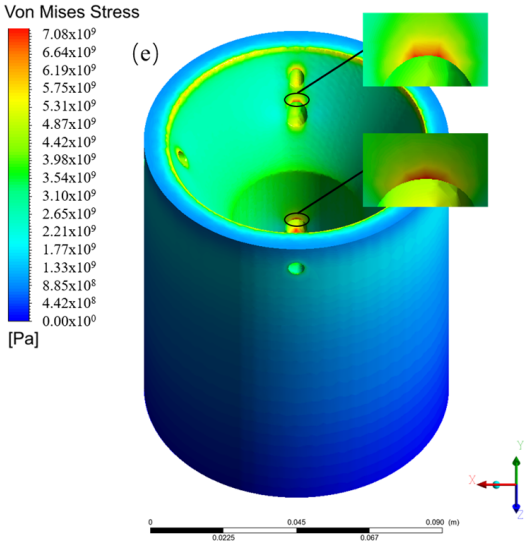

Figure 7. Thermal stress cloud of reactor under different powers. (**a**) Power of 1 kW; (**b**) power of 2 kW; (**c**) power of 3 kW; (**d**) power of 4 kW; (**e**) power of 5 kW.

6.2. Effect of the Emissivity of the Inner Wall Material of the Solar Reactor on Thermal Stress

Figure 8 illustrates the impact of emissivity on the thermal stress in a solar reactor with various inner wall materials. The calculation parameters are as follows: a gas inlet velocity of 0.005 m/s, a gas inlet temperature of 300 K, a working pressure of 0.1 MPa, and an inner wall material emissivity of 0.2~0.5. From the figure, it is evident that as the emissivity of the inner wall material of the solar reactor increases, the thermal stress at points A and B of the solar reactor also increases. The main reason is that, as the emissivity increases, the thermal diffusivity and internal energy both decrease. The decrease in internal energy leads to a decrease in temperature [31]. Additionally, the temperature decrease is further amplified by the increase in emissivity [32]. Consequently, this leads to an increase in the temperature difference inside the solar reactor and an increase in thermal stress. When the emissivity of the inner wall material of the solar reactor ranges from 0.2 to 0.5, the thermal stress at point A increases from 6.24 $\times$ 10^3 MPa to 6.58 $\times$ 10^3 MPa, and, at point B, the thermal stress increases from 6.21 $\times$ 10^3 MPa to 6.56 $\times$ 10^3 MPa. Figure 9 shows the distribution of thermal stress, in a cloud map, under different emissivity conditions in terms of the solar reactor's inner wall materials. It can be observed from the figure that increasing the emissivity of the inner wall materials of the solar reactor can improve the temperature inside the reactor. However, it can also worsen the phenomenon of thermal stress concentration in the reactor. Therefore, when selecting the emissivity of the internal materials in solar reactors, it is necessary to consider the distribution of internal temperature and issues related to stress concentration.

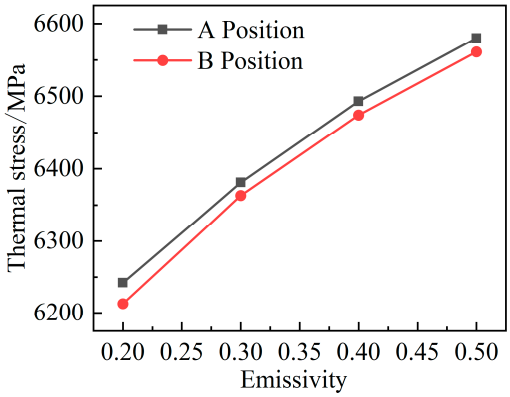

Figure 8. The influence of the emissivity of the reactor's inner wall material on thermal stress.

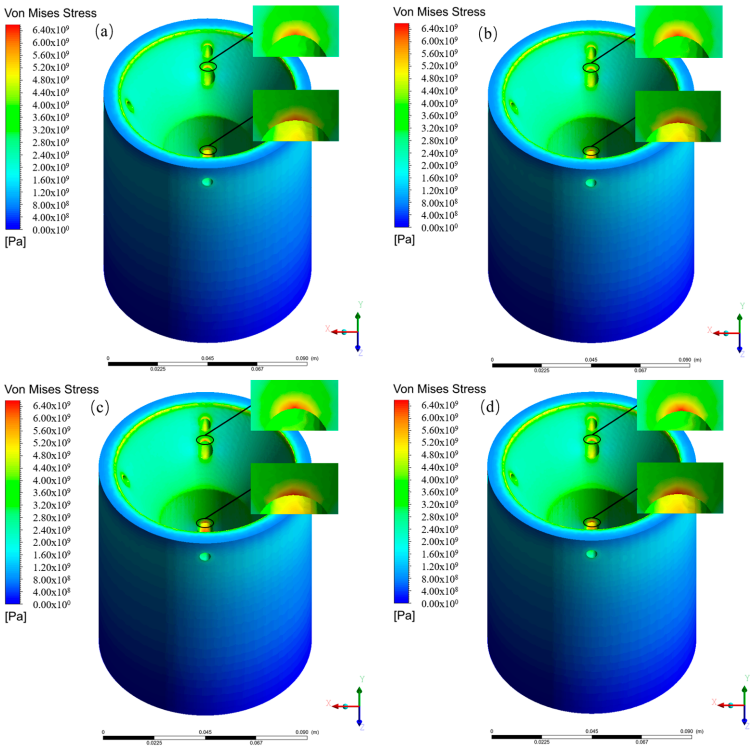

Figure 9. Thermal stress cloud diagrams under different reactor inner wall emissivities. (**a**) The emissivity is 0.2; (**b**) the emissivity is 0.3; (**c**) the emissivity is 0.4; (**d**) the emissivity is 0.5.

6.3. The Influence of Gas Inlet Velocity

Figure 10 shows the impact of various gas inlet velocities on the thermal stress of solar reactors. The calculation parameters include the impact of various gas inlet velocities on the thermal stress of the solar reactor under the following conditions: the power of the solar simulator is 2.4 kW, the gas inlet temperature is 300 K, and the working pressure is 0.1 MPa. From the figure, it can be seen that the increase in gas inlet velocity has little effect on the thermal stress of the solar reactor. Due to the minimal effect of the increase in gas inlet velocity on the internal temperature difference of the solar reactor, its impact on the thermal stress of the solar reactor is relatively insignificant. When the gas inlet velocity increased from 0.003 m/s to 0.09 m/s, the thermal stress at points A and B only decreased by 10 MPa. Figure 11 shows the cloud maps of thermal stress distribution when the gas inlet velocity increases from 0.003 m/s to 0.09 m/s. It can also be seen from the figure that the gas inlet velocity has little effect on the thermal stress in solar reactors A and B. Although the gas inlet velocity affects the temperature distribution inside the solar reactor, it does not have a significant impact on the temperature difference at the front end of the solar reactor's aperture [3]. Therefore, it is not feasible to reduce the thermal stress concentration by increasing the gas inlet velocity of the solar reactor.

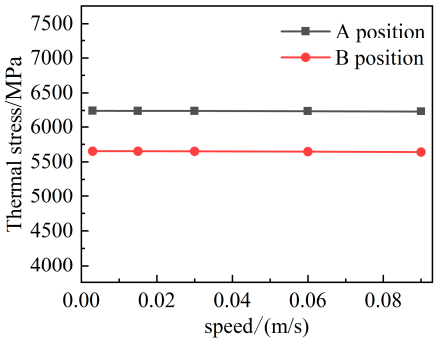

Figure 10. Effect of inlet velocity on thermal stress.

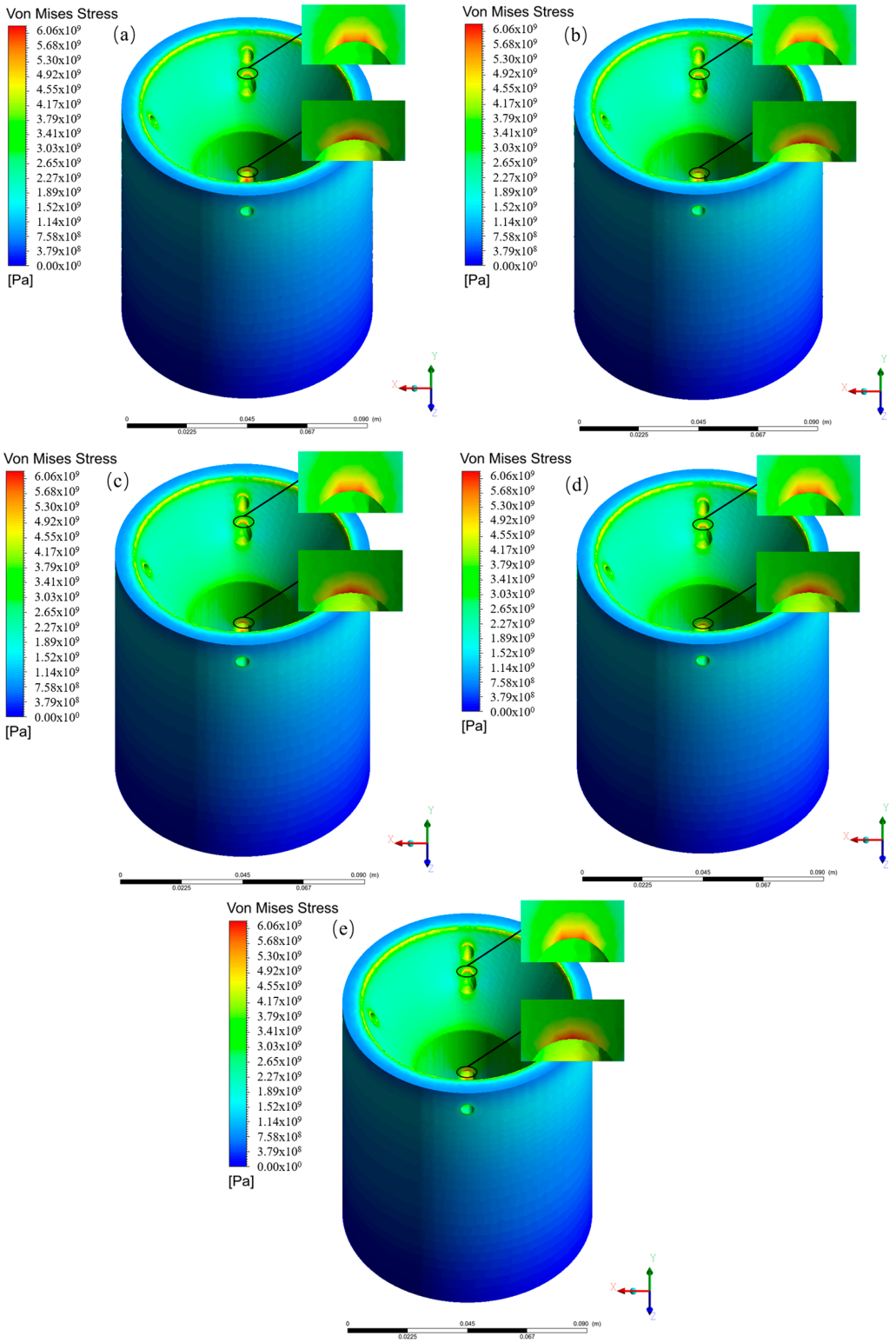

Figure 11. Thermal stress clouds of the reactor under different inlet velocities. (**a**) The inlet velocity is 0.003 m/s; (**b**) the inlet velocity is 0.015 m/s; (**c**) the inlet velocity is 0.03 m/s; (**d**) the inlet velocity is 0.06 m/s; (**e**) the inlet velocity is 0.09 m/s.

6.4. Effect of Working Pressure

Figure 12 illustrates the impact of various working pressures on the thermal stress of solar reactors. The calculation parameters are as follows for the impact of various operating pressures on the thermal stress of a solar reactor: a solar simulator power of 2.4 kW, a

gas inlet temperature of 300 K, and an inlet velocity of 0.005 m/s. From the figure, it can be seen that an increase in working pressure has little effect on the thermal stress of the solar reactor. The main reason is that, although the pressure is increased, the thermal resistance does not change with the increase in pressure [33]. Therefore, it does not cause temperature changes and generate thermal stress. When the working pressure increased from 0.1 MPa to 2 MPa, the thermal stress at points A and B only decreased by 10 MPa. Figure 13 shows the cloud diagrams of the thermal stress distributions in solar reactors under working pressures ranging from 0.1 MPa to 2 MPa. It can also be seen from the figure that the working pressure has little effect on stress concentrations. Although the working pressure does affect the temperature distribution of the solar reactor, its impact on the internal temperature difference is relatively small. Thus, it cannot reduce thermal stress. Therefore, it is not feasible to reduce thermal stress concentrations by changing the operating pressure of the solar reactor.

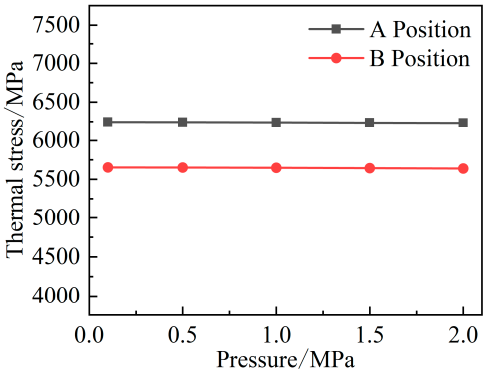

Figure 12. Influence of working pressure on thermal stress.

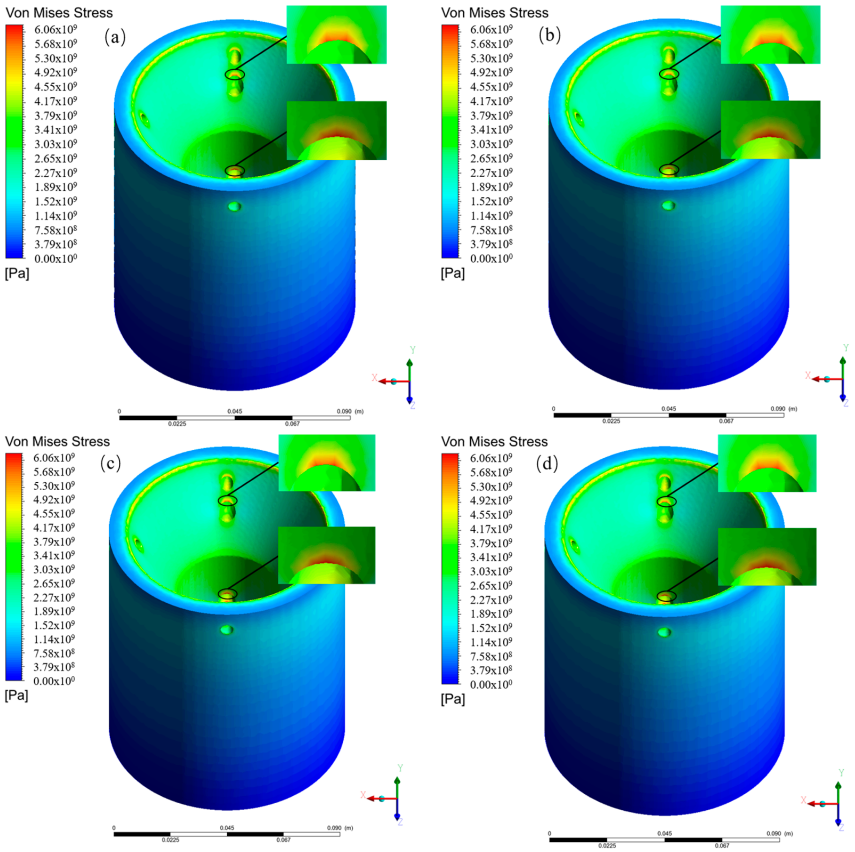

Figure 13. *Cont.*

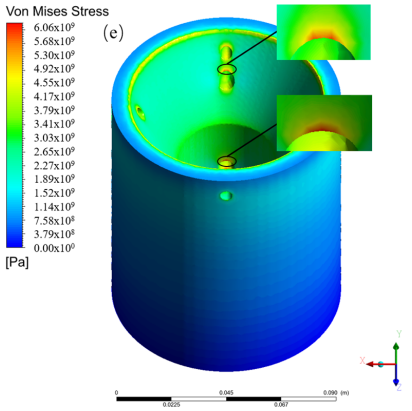

Figure 13. Thermal stress clouds of the reactor under different working pressures. (**a**) The working pressure is 0.1 MPa; (**b**) the working pressure is 0.5 MPa; (**c**) the working pressure is 1 MPa; (**d**) the working pressure is 1.5 MPa; (**e**) the working pressure is 2 MPa.

6.5. Effect of Thermocouple Aperture Diameter on Solar Reactor

Figure 14 illustrates the impact of the diameter of the thermocouple opening at the center of the porous area in various solar reactors on the thermal stress experienced by the solar reactor. Under the condition that the diameter of the thermocouple opening in the front of the solar reactor remains unchanged, the calculation parameters are as follows for the influence of the diameter of the thermocouple opening at the center of different porous areas on the thermal stress at point A of the solar reactor: the power of the solar simulator is 2.4 kW, the gas inlet temperature is 300 K, the gas inlet speed is 0.005 m/s, and the working pressure is 0.1 MPa. From Figure 14, it can be observed that as the diameter of the thermocouple opening in the center of the porous area increases, the thermal stress at point A also increases. When the diameter of the thermocouple opening at the center of the porous area increases from 3 mm to 7 mm, the thermal stress at point A increases from 5.43×10^3 MPa to 6.24×10^3 MPa, resulting in an increase of 810 MPa. Furthermore, the rate of increase in the curve gradually slows down. This is due to the smaller aperture blocking incident radiation [34]. As the aperture increases, radiation heat transfer is enhanced, reducing fluid phase resistance [35]. This results in a temperature rise and the formation of a larger temperature gradient, leading to an increase in thermal stress. Figure 15 shows the thermal stress cloud maps of the solar reactor with varying diameters of thermocouple openings at the center of its porous area. It can be observed from the figure that as the diameter of the thermocouple openings at the center of the various porous areas increases, the thermal stress at point A also increases. The rise in thermal stress significantly impacts solar reactors. Thermocouples are crucial for measuring the temperature of the porous area in solar reactors. The minimum diameter of the thermocouples commonly available on the market can reach 2 mm. Therefore, when designing the diameter of the thermocouple in the center of the porous area of a solar reactor, it is necessary to choose a smaller thermocouple diameter to minimize thermal stress.

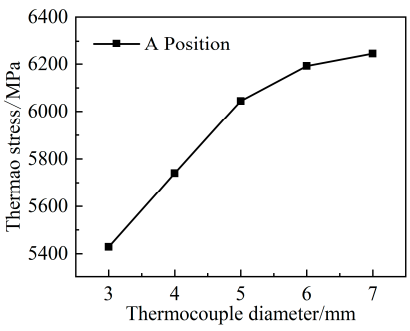

Figure 14. Influence of thermocouple diameter on thermal stress.

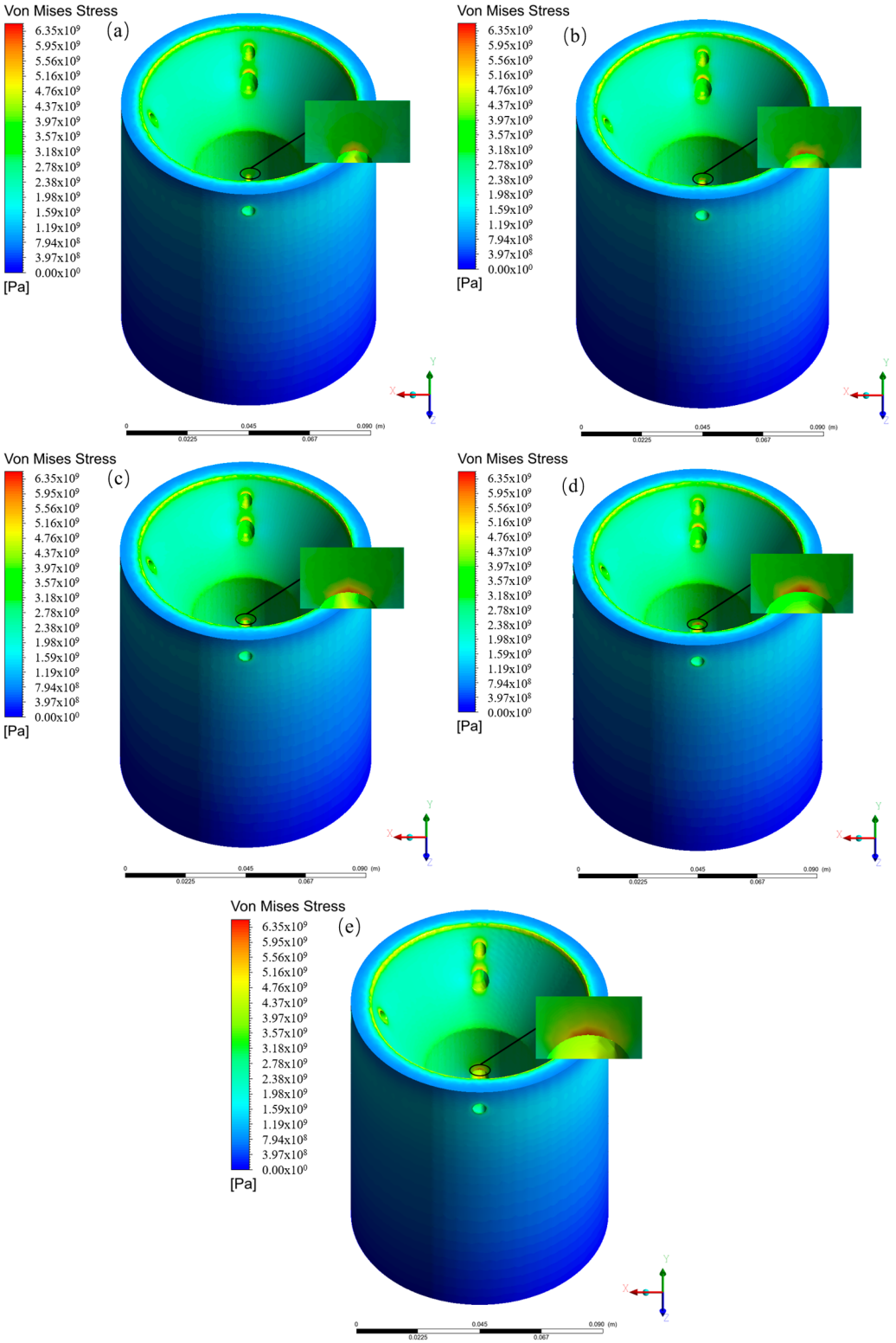

Figure 15. Thermal stress cloud diagrams of reactors with different thermocouple diameters. (**a**) The thermocouple diameter is 3 mm; (**b**) the thermocouple diameter is 4 mm; (**c**) the thermocouple diameter is 5 mm; (**d**) the thermocouple diameter is 6 mm; (**e**) the thermocouple diameter is 7 mm.

7. Conclusions

In this chapter, a solar thermochemical reactor was designed based on a 5 kW non-coaxial concentrating solar simulator, and a thermal stress analysis model of the reactor was established. The model was used to study the influence of solar simulator power,

solar reactor inner wall material emissivity, working pressure, gas inlet velocity, and thermocouple opening diameter on the thermal stress of the solar reactor. By adjusting various operating conditions of the solar reactor, it is possible to reduce the phenomenon of thermal stress concentration, thereby enhancing the stability and lifespan of the reactor. At present, there has been no consideration of the effect of thermochemical reactions on thermal stress. Therefore, the next step for research could be focusing on investigating thermochemical reactions. Our main conclusions are as follows:

(1) As the power of the solar simulator increases, the thermal stress on the solar reactor also increases. This is primarily attributed to the rise in power, which results in wall radiation heat loss. Consequently, temperature non-uniformity is induced, further intensifying the concentration of thermal stress.

(2) Increasing the emissivity of the inner wall material of the solar reactor leads to an increase in thermal stress. This is mainly because as the emissivity increases, the thermal diffusivity and internal energy of the reactor decrease, leading to a decrease in temperature and exacerbating the phenomenon of thermal stress concentration.

(3) By comparing the influence of different working pressures on the thermal stress of the solar reactor, it has been demonstrated that altering the working pressure does not effectively reduce the phenomenon of thermal stress concentration. This is mainly because an increase in pressure does not generate a change in thermal resistance, thus it will not cause temperature variations and generate thermal stress.

(4) By comparing the effects of different inlet velocities on the thermal stress of the solar reactor, it was proven that changing the gas inlet velocity does not effectively reduce the concentration of thermal stress. Mainly, the inlet velocity has an impact on the internal temperature distribution of the solar reactor, but it does not significantly affect the temperature difference at the front end of the solar reactor's aperture.

(5) By comparing the influence of different thermocouple opening diameters on thermal stress, it was concluded that using a smaller thermocouple opening diameter can reduce the thermal stress inside the solar reactor. This is because the smaller aperture blocks incident radiation. As the aperture increases, the radiation heat transfer strengthens, reducing fluid phase resistance. This causes a temperature rise and forms a larger temperature gradient, leading to an increase in thermal stress.

Author Contributions: Methodology, X.Y. and H.Z.; Formal Analysis, F.G. and Y.L. (Yan Lin); Writing—original draft, X.H. and Y.L(Yan Lin).; Writing—review and editing, X.Y. and Y.L (Yang Liu). All authors have read and agreed to the published version of the manuscript.

Funding: This work was supported by the National Natural Science Foundation of China (52374336), Hebei Province High School Science Research Project (BJK2024058), Youth Scholars Promotion Plan of North China University of Science and Technology (QNTJ202205), Applied Basic Research Project of Tangshan (22130233H), and the Talent Foundation of Tangshan (A202110039).

Data Availability Statement: Data are contained within the article.

Conflicts of Interest: Author Xin Yao was employed by the company Tangshan Chuangyuan Fangda Electric Co., Ltd. The remaining authors declare that the research was conducted in the absence of any commercial or financial relationships that could be construed as a potential conflict of interest.

References

1. Abdelrazik, A.S.; Osama, A.; Allam, A.N.; Shboul, B.; Sharafeldin, M.A.; Elwardany, M. ANSYS-Fluent numerical modeling of the solar thermal and hybrid photovoltaic-based solar harvesting systems. *J. Therm. Anal. Calorim.* **2023**, *148*, 11373–11424. [CrossRef]
2. Romero, M.; Steinfeld, A. Concentrating solar thermal power and thermochemical fuels. *Energy Environ. Sci.* **2012**, *5*, 9234–9245. [CrossRef]
3. Roman, B.; Rohini, B.C.; Venstrom, L.J.; Stephen, J.S.; Peter, T.K. Design of a Solar Reactor to Split CO_2 Via Isothermal Redox Cycling of Ceria. *J. Sol. Energy Eng.* **2015**, *137*, 031007.
4. Rajendran, D.R.; Ganapathy Sundaram, E.; Jawahar, P.; Vathilingam, S.; Omid, M. Review on influencing parameters in the performance of concentrated solar power collector based on materials, heat transfer fluids and design. *J. Therm. Anal. Calorim.* **2020**, *140*, 33–51. [CrossRef]

5. Mohammed, A.H.; Shmroukh, A.N.; Ghazaly, N.M.; Kabeel, A.E. Active solar still with solar concentrating systems, Review. *J. Therm. Anal. Calorim.* **2023**, *148*, 8777–8792. [CrossRef]
6. Kurkute, N.; Priyam, A. A thorough review of the existing concentrated solar power technologies and various performance enhancing techniques. *J. Therm. Anal. Calorim.* **2022**, *147*, 14713–14737. [CrossRef]
7. Lipiński, W.; Davidson, J.H.; Haussener, S.; Klausner, J. Review of heat transfer research for solar thermochemical applications. *J. Therm. Sci. Eng. Appl. Appl.* **2013**, *5*, 021005. [CrossRef]
8. Xu, D.; Liu, Q.B.; Lei, J.; Jin, H.G. Performance of a combined cooling heating and power system with mid-and-low temperature solar thermal energy and methanol decomposition integration. *Energy Convers. Manag.* **2015**, *102*, 17–25. [CrossRef]
9. Likkasit, C.; Maroufmashat, A.; Elkamel, A.; Ku, H.M.; Fowler, M. Solar-aided hydrogen production methods for the integration of renewable energies into oil & gas industries. *Energy Convers. Manag.* **2018**, *168*, 395–406.
10. Ebadi, M.; Mehrpooya, M.; Kani, A.H. Sensitivity analysis and optimization of geometric and operational parameters in a thermochemical heat storage redox reactor used for concentrated solar power plants. *J. Therm. Anal. Calorim.* **2022**, *147*, 6415–6435. [CrossRef]
11. Li, L.; Chen, C.; Singh, A.; Rahmatian, N.; Nick, A.Y.; Randhir, K.; Mei, R.; James, F.K.; David, W.H.; Pereasch, J. A transient heat transfer model for high temperature solar thermochemical reactors. *Int. J. Hydrogen Energy* **2016**, *41*, 2307–2325. [CrossRef]
12. Dake, L.S.; Lind, M.A.; Maag, C.R. *A Comparison of the Effect of Outdoor Exposure on the Optical Properties of Solar Mirrors and Transparent Encapsulant Materials Technical Report No. PNL-4074 UC-62*; Pacific Northwest Laboratory: Richland, WA, USA, 1981.
13. Dake, L.S.; Lind, M.A. *The Optical Losses of Solar Mirrors Due to Atmospheric Contamination at Liberal, Kansas and Oologah, Oklahoma, Technical Report No. PNL-4073 UC-62*; Pacific Northwest Laboratory: Richland, WA, USA, 1981.
14. Bethea, R.M.; Barriger, M.T.; Williams, P.F.; Chin, S. Environmental effects on solar concentrator mirrors. *Sol. Energy* **1981**, *27*, 497–511. [CrossRef]
15. Berry, M.; Dursch, H. Exposure testing of solar collector plastic films. *Sol. Energy Mater.* **1980**, *3*, 247–261. [CrossRef]
16. Schissel, P.; Czanderna, A.W. Reactions at the silver/polymer interface: A review. *Sol. Energy Mater.* **1980**, *3*, 225–245. [CrossRef]
17. García-Segura, A.; Fernández-García, A.; Ariza, M.J.; Sutter, F.; Valenzuela, L. Durability studies of solar reflectors: A review. *Renew. Sustain. Energy Rev.* **2016**, *62*, 453–467. [CrossRef]
18. Daabo, A.M.; Mahmoud, A.; Al-Dadah, R.K.; Ahmad, A. Numerical investigation of pitch value on thermal performance of solar receiver for solar powered Brayton cycle application. *Energy* **2017**, *119*, 523–539. [CrossRef]
19. Wang, F.Q.; Shuai, Y.; Yuan, Y.; Yang, Y.; Tan, H.P. Thermal stress analysis of eccentric tube receiver using concentrated solar radiation. *Sol. Energy* **2010**, *84*, 1809–1815. [CrossRef]
20. Wang, F.Q.; Shuai, Y.; Yuan, Y.; Liu, B. Effects of material selection on the thermal stresses of tube receiver under concentrated solar irradiation. *Mater. Des.* **2012**, *33*, 284–291. [CrossRef]
21. Du, S.; Wang, Z.; Shen, S. Thermal and structural evaluation of composite solar receiver tubes for Gen3 concentrated solar power systems. *Renew. Energy* **2022**, *189*, 117–128. [CrossRef]
22. Hischier, I.; Poživil, P.; Steinfeld, A. A modular ceramic cavity-receiver for high- temperature high-concentration solar applications. *J. Sol. Energy Eng.* **2012**, *134*, 011004. [CrossRef]
23. Chen, Y.X.; Wang, D.; Zou, C.Z.; Gao, W.; Zhang, Y.P. Thermal performance and thermal stress analysis of a supercritical CO2 solar conical receiver under different flow directions. *Energy* **2022**, *246*, 123344. [CrossRef]
24. Zhang, H.; Shuai, Y.; Bachirou, G.L.; Jiang, B.S. Thermal characteristics and thermal stress analysis of solar thermochemical reactor under high-flux concentrated solar irradiation. *Sci. China Technol. Sci.* **2020**, *63*, 1776–1786. [CrossRef]
25. Zou, Y.; Qin, C.Y.; Liu, H.T.; Zhang, B.; Wu, X.H. Concentrating photovoltaic systems: A review of temperature effects and components. *J. Therm. Anal. Calorim.* **2023**, *149*, 1301–1329. [CrossRef]
26. Wan, Z.J.; Fang, J.B.; Tu, N.; Wei, J.J.; Qaisrani, M.A. Numerical study on thermal stress and cold startup induced thermal fatigue of a water/steam cavity receiver in concentrated solar power (CSP) plants. *Sol. Energy* **2018**, *170*, 430–441. [CrossRef]
27. Conroy, T.; Collins, M.N.; Grimes, R. A review of steady-state thermal and mechanical modelling on tubular solar receivers. *Renew. Sustain. Energy Rev.* **2020**, *119*, 109591. [CrossRef]
28. Sedighia, M.; Padillaa, R.V.; Taylorb, R.A.; Lake, M.; Izadgoshasb, I.; Rose, A. High-temperature point-focus pressurised gas-phase solar receivers: A comprehensive review. *Energy Convers. Manag.* **2019**, *185*, 678–717. [CrossRef]
29. Lougou, B.G.; Shuai, Y.; Xing, H.; Yuan, Y.; Tan, H.P. Thermal performance analysis of solar thermochemical reactor for syngas production. *Int. J. Heat Mass Transf.* **2017**, *111*, 410–418. [CrossRef]
30. Lougou, B.G.; Shuai, Y.; Chen, X.; Yuan, Y.; Tan, H.P.; Xing, H. Analysis of radiation heat transfer and temperature distributions of solar thermochemical reactor for syngas production. *Front. Energy* **2017**, *11*, 480–492. [CrossRef]
31. Lougou, B.G.; Shuai, Y.; Pan, R.; Chaffa, G.; Tan, H.P. Heat transfer and fluid flow analysis of porous medium solar thermochemical reactor with quartz glass cover. *Int. J. Heat Mass Transf.* **2018**, *127*, 61–74. [CrossRef]
32. Villafán-Vidales, H.I.; Abanades, S.; Caliot, C.; Romero-Paredes, H. Heat transfer simulation in a thermochemical solar reactor based on a volumetric porous receiver. *Appl. Therm. Eng.* **2011**, *31*, 3377–3386. [CrossRef]
33. Wang, M.; Siddiqui, K. The impact of geometrical parameters on the thermal performance of a solar receiver of dish-type concentrated solar energy system. *Renew. Energy* **2010**, *35*, 2501–2513. [CrossRef]

34. Chandran, R.B.; De Smith, R.M.; Davidson, J.H. Model of an integrated solar thermochemical reactor/reticulated ceramic foam heat exchanger for gas-phase heat recovery. *Int. J. Heat Mass Transf.* **2015**, *81*, 404–414. [CrossRef]
35. Besarati, S.M.; Goswami, D.Y.; Stefanakos, E.K. Development of a solar receiver based on compact heat exchanger technology for supercritical carbon dioxide power cycles. *J. Sol. Energy Eng.* **2015**, *137*, 031018. [CrossRef]